Optical Extinction Measurements of Dust Density in the GMRO Regolith Test Bin

J. Lane[1], J. Mantovani[2], R. Mueller[2], M. Nugent[1], A. Nick[1], J. Schuler[1], and I. Townsend[1]

[1]ESC, Granular Mechanics and Regolith Operations Lab, ESC-58, Kennedy Space Center, FL 38299; [2]NASA, Granular Mechanics and Regolith Operations Lab, NE-S Kennedy Space Center, FL 38299

ABSTRACT

A regolith simulant test bin was constructed and completed in the Granular Mechanics and Regolith Operations (GMRO) Lab in 2013. This Planetary Regolith Test Bed (PRTB) is a 64 $m^2 \times 1$ m deep test bin, is housed in a climate-controlled facility, and contains 120 MT of lunar-regolith simulant, called Black Point-1 or BP-1, from Black Point, AZ. One of the current uses of the test bin is to study the effects of difficult lighting and dust conditions on Telerobotic Perception Systems to better assess and refine regolith operations for asteroid, Mars and polar lunar missions. Low illumination and low angle of incidence lighting pose significant problems to computer vision and human perception. Levitated dust on Asteroids interferes with imaging and degrades depth perception. Dust Storms on Mars pose a significant problem. Due to these factors, the likely performance of telerobotics is poorly understood for future missions. Current space telerobotic systems are only operated in bright lighting and dust-free conditions. This technology development testing will identify: (1) the impact of degraded lighting and environmental dust on computer vision and operator perception, (2) potential methods and procedures for mitigating these impacts, (3) requirements for telerobotic perception systems for asteroid capture, Mars dust storms and lunar regolith ISRU missions.

In order to solve some of the Telerobotic Perception system problems, a plume erosion sensor (PES) was developed in the Lunar Regolith Simulant Bin (LRSB), containing 2 MT of JSC-1a lunar simulant. PES is simply a laser and digital camera with a white target. Two modes of operation have been investigated: (1) *single laser spot* – the brightness of the spot is dependent on the optical extinction due to dust and is thus an indirect measure of particle number density, and (2) *side-scatter* – the camera images the laser from the side, showing beam entrance into the dust cloud and the boundary between dust and void. Both methods must assume a mean particle size in order to extract a number density. The optical extinction measurement

Fig. 1. NASA worker in the PRTB performing soil penetration testing.

yields the product of the 2nd moment of the particle size distribution and the extinction efficiency Q_e. For particle sizes in the range of interest (> 1 μm), $Q_e \approx 2$. Scaling up of the PES single laser and camera system is underway in the PRTB, where an array of lasers penetrate a controlled dust cloud, illuminating multiple targets. Using high speed HD GoPro video cameras, the evolution of the dust cloud and particle size density can be studied in detail.

BACKGROUND: PLUME EROSION SENSOR

Improved methods for measuring plume erosion rates during landing of spacecraft on the moon are needed. These rates are necessary for estimating potential impacts from surface ablation during future Google X-Prize landings on the Moon. Some of the landings will take place near Apollo sites, which may be sandblasted as Google X-Prize spacecraft land nearby. Recent photogrammetric studies combined with modeling of the processes of erosion gave initial estimates of erosion rates during Apollo landings, however, with large uncertainty (Immer et al, 2011; Lane and Metzger, 2014).

The problem of using a laser to measure ejected dust density during a lunar lander descent was investigated and studied. The PES was developed for this purpose. The instrument's laser brightness is attenuated according to dust density and extinction. The camera images the laser and associated beam attenuation. Two configurations were studied, as described above: (1) *laser spot* and (2) *side scatter*, where the laser is imaged for some distance into the cloud before it either leaves the camera's field of view or it is attenuated beyond detection. Each method must be able to image the laser spot or beam with a minimum of several pixels across the laser beam diameter. This is an important issue with camera and lens magnification, distance to the beam or spot, and intensity of the beam or spot as compared to the sun. Both methods have additional pros and cons.

The laser spot method involves a simpler geometry and fewer assumptions need to be made in analyzing the data. The disadvantage is that the laser spot will be attenuated beyond detection, even under modest conditions, and regardless of practical laser power. This method is useful for low density particle numbers where $N < 10^{10}$ [m^{-3}], and/or for small mean particle sizes where $D < 10$ [μm]. This would occur for example when the rocket nozzle is still many meters above the surface and when the engine is shutting down. The side scatter configuration is useful for the conditions where the laser spot is obscured, such as large particle size and/or high density. A disadvantage of the side scatter method is more difficulty in analysis and difficulty in aligning the laser and camera to acquire useful data.

In general, the larger the laser power the better, there is really no physical reason why there would be too much laser power. The power limit is based on practical considerations, such as weight and size. Camera imager gain must be scaled with the laser intensity, otherwise the image pixel values could be either saturated or too dark. If the camera, laser, and dust are all in shadow, then the dynamic range of the camera can in theory be matched to the laser power to "see" deeper into the cloud. In practice, the cloud will be illuminated by the sun and the albedo of this cloud will be similar to and possibly greater than the albedo of the lunar surface. This effect is the biggest problem with the laser spot method, and even though it will also affect the side scatter method, attenuation as a function of laser depth should be measurable from the side under most sunlit conditions.

Conceptually, the PES attempts to derive microphysical properties of plumes of lunar dust from images taken during landing. The sensor consists of red or green lasers and a video camera mounted on the landing spacecraft. The laser beams are arranged within the field of view (FOV) of either video or photographic cameras. The cameras will record images of a dust plume intersecting the path of the laser beams and the intensity of scattered radiation will be analyzed and used to derive particle density, which is needed for accurately estimating erosion rates of lunar regolith. As the landing craft descends, a plume of dust is created when rocket thrust reaches the height to touchdown above the moon. This height will be dependent on the thrust and dimensions of the lander. The lasers will be aimed at the height to touchdown (14 m). During landing, the plume of dust will intersect the path of the lasers and the intensity of radiation scattered into FOV of the camera will be a function of the density of particles of the beam, the distance from the beam, and the view angle of the camera. Particle density will be derived from an extinction coefficient obtained from the attenuation of the laser beam through the dust plume. The camera will have a fixed focus and thus a fixed resolution. In order for a camera to distinguish a green/red spot on the surface of the moon, the intensity of the reflected laser radiation from the surface of the Moon would have to exceed the reflected solar radiation into the FOV of the camera. A further correction for each laser must be made for either the R or G bands from an RGB format. The size of the spot must also be larger than a square of 2 pixels square. An analysis of laser power requirements was made to size and cost a laser system for the PES.

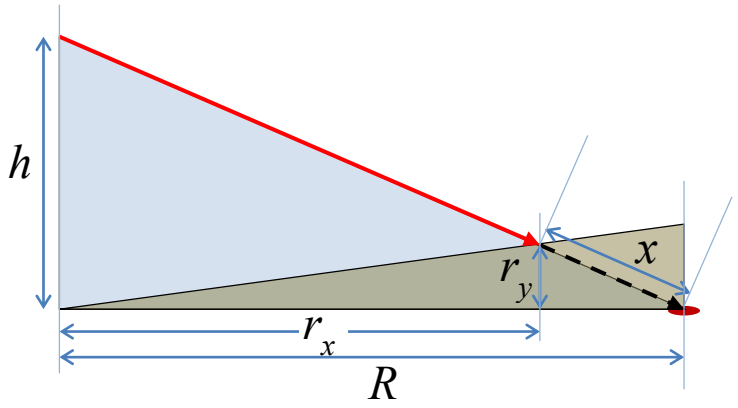

Fig. 2. Simplified schematic of laser geometry. The laser is located h above the surface and is projected through a dust sheet of angle $\theta = \tan^{-1}(r_y/r_x)$. The laser spot is attenuated along the path length x through the dust sheet. The reflection back to the camera is again attenuated by another distance x'.

The requirements for viewing and measuring the intensity of a laser spot projected onto the lunar surface have been discussed in the previous section. The important parameters include spot size, pixel resolution and range from the camera to the surface. In addition, a laser spot needs to be equally intense or greater than the background illumination from the sun. Once these requirements have been met to view an un-obscured laser spot, the next consideration is attenuation of the laser spot due to optical extinction.

Consider the geometry of a laser projecting a spot from a distance h above the surface in Figure 2. The dust angle is $\theta = \tan^{-1}(r_y/r_x)$. The extinction path distance x due to the dust cloud is:

$$x = \frac{R \tan\theta \left(h^2+R^2\right)^{1/2}}{h + R \tan\theta} \quad (1)$$

As an example, for h = 2 [m], R = 5 [m], and θ = 3°, then from Equation (1), x = 0.62 [m].

EXPERIMENTS IN LSRB

The extinction factor ε is dependent on the density of particles in the cloud N, and particle average size $\overline{D}$, as well as the path length x:

$$\varepsilon = e^{-\beta x} \quad (2)$$

where $\beta = \sigma N$, and the scattering cross-section $\sigma = \pi Q_e \overline{D}^2/4$. Table 1 lists several measurements of $\overline{D}$, providing a range of values from which to estimate the particle density N.

Table 1. Average particle diameter [μm], based on 2nd moment of distribution of JSC-1a.

GMRO Lab Experiments				Fine particle Analyzer			
37	60	40	29	50	70	73	36

Particle number density N [m^{-3}] can be estimated from lab experiments as well, using the measured mass transfer rate $\dot{m}$ [kg/s]:

$$N = \frac{24\,\dot{m}}{\pi^2 D_p^2 \overline{D}^3 \bar{v}\, \rho_p} \quad (3)$$

where D_p is the particle stream diameter (of the experiment), $\bar{v}$ is the average velocity of the particles, and ρ_p is the particle bulk density (≈ 3100 kg m^{-3}). In the lab experiments, corresponding to Table 1, several values of mass transfer were used, shown in Table 2.

Table 2. Mass transfer rate and average particle velocity used in GMRO lab experiments.

	Exp #1	Exp #2	Exp #3
$\dot{m}$ [kg s^{-1}]	0.0125	0.025	0.037
$\bar{v}$ [m s^{-1}]	17.7	31.1	31.1

Table 3. Particle density N [m^{-3}] from Equation (3).

Particle diameter from Table 1	37	60	40	29
Exp #1	1.70×10^{10}	3.98×10^{9}	1.34×10^{10}	3.52×10^{10}
Exp #2	1.93×10^{10}	4.52×10^{9}	1.53×10^{10}	4.01×10^{10}
Exp #3	2.86×10^{10}	6.70×10^{9}	2.26×10^{10}	5.93×10^{10}

The extinction coefficient for the range of values in these lab experiments is plotted in Figure 3 using Equations (2), where x is the round trip path distance. The extinction coefficient falls rapidly towards zero for particle density larger than 10^{10} [m^{-3}], and for particle diameter much larger than 10 μm.

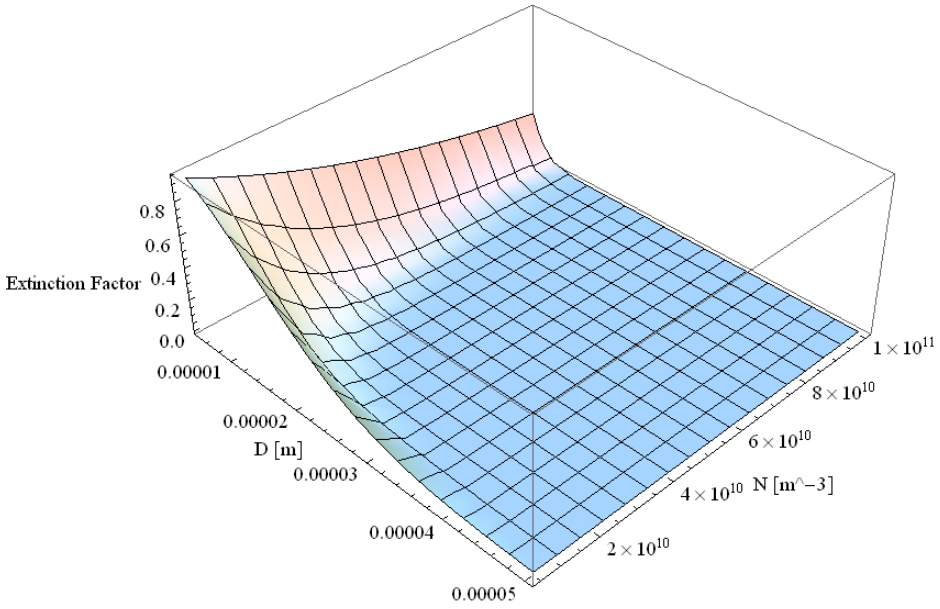

Fig. 3. Extinction coefficient from Equation (2), with x = 0.62 [m].

This result implies that a laser spot on the surface can only be viewed under a limited set of conditions. This will be discussed in more detail in the Summary section. Practical conditions where dust density measurements are meaningful using a laser spot are limited to low particle density and mean particle size. For this reason, side scatter extinction measurements will yield results under a larger range of conditions.

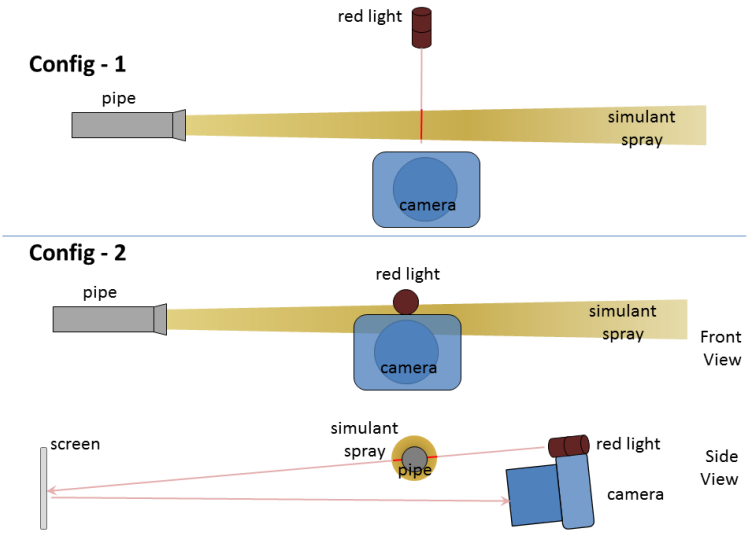

Fig. 4. Side scatter (top) and single spot (bottom) configurations.

The following figures show *Exp #1*, performed in the GMRO lab, where a laser spot was projected through a 2.54 [cm] diameter particle stream. The first image corresponds to *Configuration-1*, while the next two correspond to *Configuration-2*. Using Equation (2), the number density *N*, was estimated from taking the ratio of luminosity difference values (subtracting out background luminosity) of the laser spot with and without dust.

Fig. 5. Side-scatter measurement.

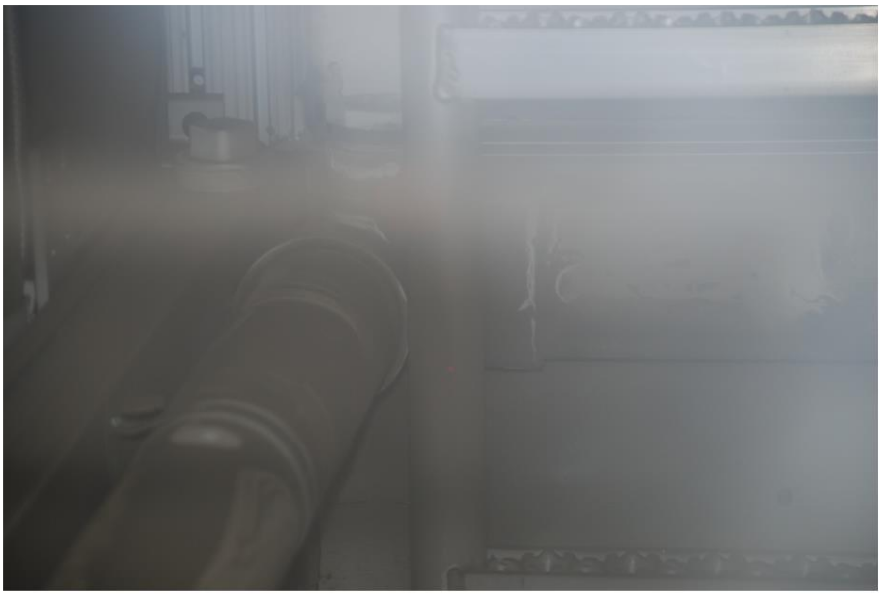

with dust

Fig. 5. Single spot measurement: with dust (top); without dust (bottom).

EXPERIMENTS IN THE PRTB

The key difference in the PRTB testing as compared to the LSRB, is the introduction of a laser array. This variable angle – 9 laser pointer (VA9LP) fixture provides quick adjustment to the direction of each individual laser. The fixture element consists of two parallel 12" x 12" sheets of 3/8" birch wood. Each sheet of wood has 9 holes cut in it, in a 3 x 3 pattern. The holes are larger than the laser body diameter *D* by approximately a factor of two. Each laser is inserted through a hole cut through a rubber sphere so that the laser fits snugly in the ball. The ball diameter is chosen to be about 3 times the diameter of the laser. The ratio of ball diameter to hole diameter in sheet to hole diameter though the ball is approximately 3*D*:2*D*:*D*. This design allows balls to be rotated through a solid angle of approximately π, which provides extreme flexibility in pointing the lasers for a variety of application. In this specific case, the desire is to aim the 9 lasers at 9 targets on the back wall of the Regolith Test Bin.

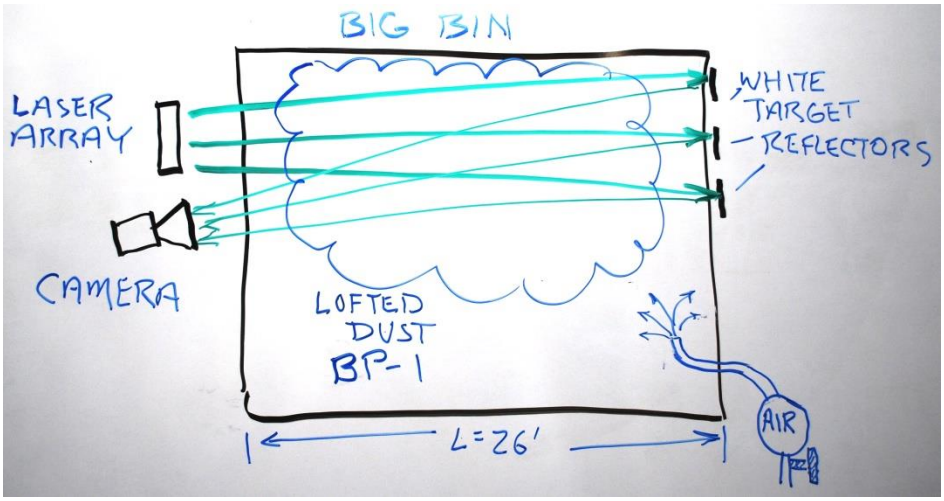

Fig. 6. PRTB setup with multiple lasers.

Figure 6 shows a setup in PRTB used to test the system. Figure 7 is a view from the side at a small oblique angle which reveals the laser side scatter. In Figure 7, the length of the laser lines extends over the 26 ft distance from front wall to the back wall, even though the laser beams may fade in the image before reaching the back wall. Another challenge in analyzing this image is the multiple reflections seen from the front and back walls, which show up as bright spots.

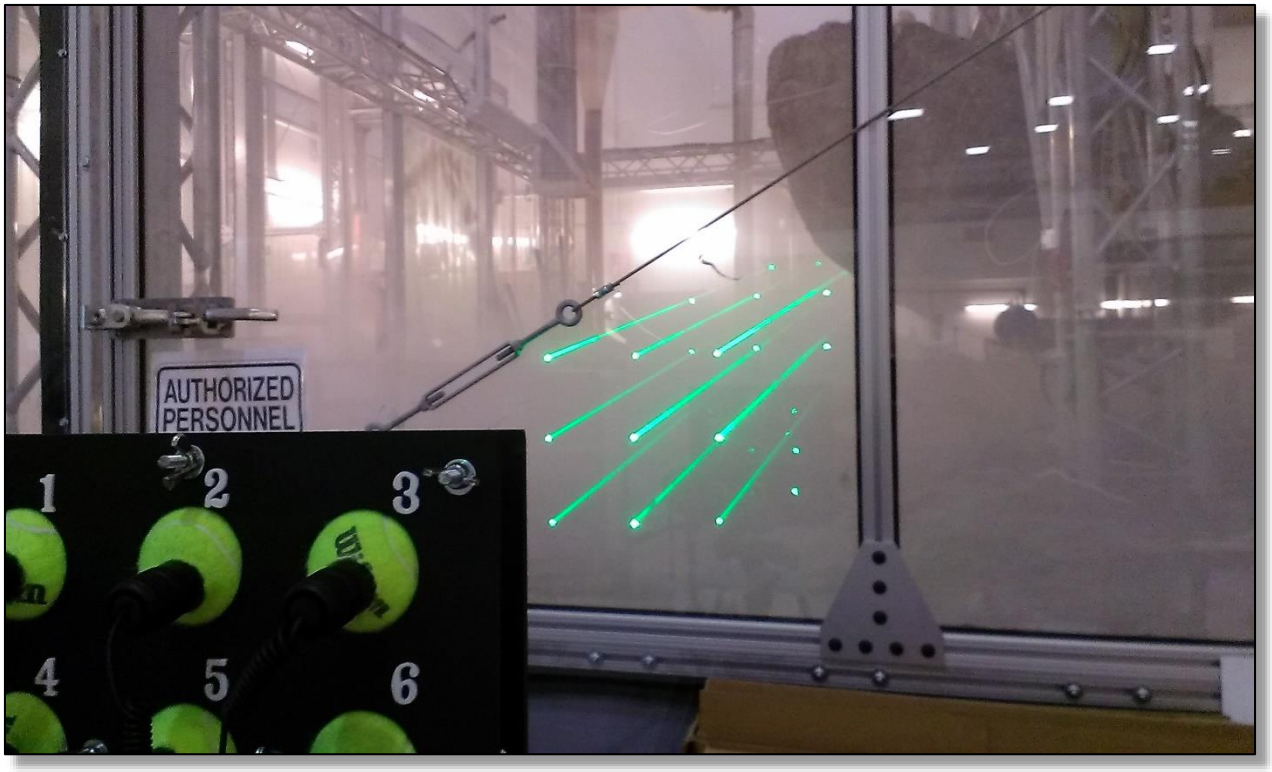

Fig. 7. PRTB showing laser side-scatter.

Figure 8 shows the single laser spots that are used in the data analysis of this paper (side-scatter data will be reported at a later time). Figure 8 is essentially the same small oblique angle view (from the left side) as shown in Figure 7, but the bin is clear of dust so the side scatter beams do not appear. In Figure 8, the 9 targets on the back wall are shown with the corresponding laser spots. Bright spots in the foreground bottom right are reflected laser light from the laser array. Each time the laser beam penetrates a plastic wall, approximately 10% of the beam is reflected back from the surface.

Rewriting the optical extinction factor from Equation (2), the intensity of reflected beam from the back wall target is:

$$I(x) = I_0 e^{-\pi Q_e \alpha x/4} \tag{4}$$

We can compute the extinction coefficient in the images by measuring the intensity of the 9 laser spots in an image using an image processing program such as Adobe Elements™ . In Equation (4), $I(x)$ where $x = 2L$, is the intensity of the green channel, which has integer values from 0 to 2^8-1, as measured by the image processing software. I_0 is the intensity of the green channel for the no dust condition, such as that in Figure 8. The value of I_0 must be less than 255, otherwise

image saturation has occurred. If saturation occurs in no dust case, then Equation (5) cannot be used to determine optical density. Side scatter analysis does allow saturation to occur at some point along the laser beam line, as long as there are enough non-saturated pixels to provide an analysis.

$$\alpha = -\frac{4}{\pi Q_e x} \ln\left(\frac{I(x)}{I_0}\right) \tag{5}$$

where Q_e = extinction efficiency (≈ 2) and x = total optical distance = $2L$ (where L is bin width ≈ 7.9 m). The extinction coefficient determined in Equation (5) is related to the 2nd moment of the particle size distribution:

$$\alpha = \int_0^\infty D^2 N(D) dD \tag{6}$$

where D = particle diameter [m] and $N(D)$ = particle size distribution [m^{-3} m^{-1}].

Fig. 8. PRTB showing single spot on targets on back wall. Dots in the foreground bottom right, are reflected laser light from the laser array. Each time the laser beam penetrates a plastic wall, approximately 10% of the beam is reflected back from the surface.

A 45 s run of data was analyzed by turning on the air hose supply shown at the bottom right of Figure 6, and allowed to run for 2 min. A sequence of still pictures (once every 2 s) were taken with a Nikon D80 with settings: f = 135 mm, exposure time = 1/40 s, and F-number = F/32. Using the procedures described above to determine the values of I_0 and $I(x)$, the extinction coefficient as defined by Equation (5) were computed and plotted in Figure 9. Figure 10 shows 2D

plots of dust density as it evolves over the 45 s test. After the air hose was turned off, the dust slowly cleared and after 1 hour was mostly clear.

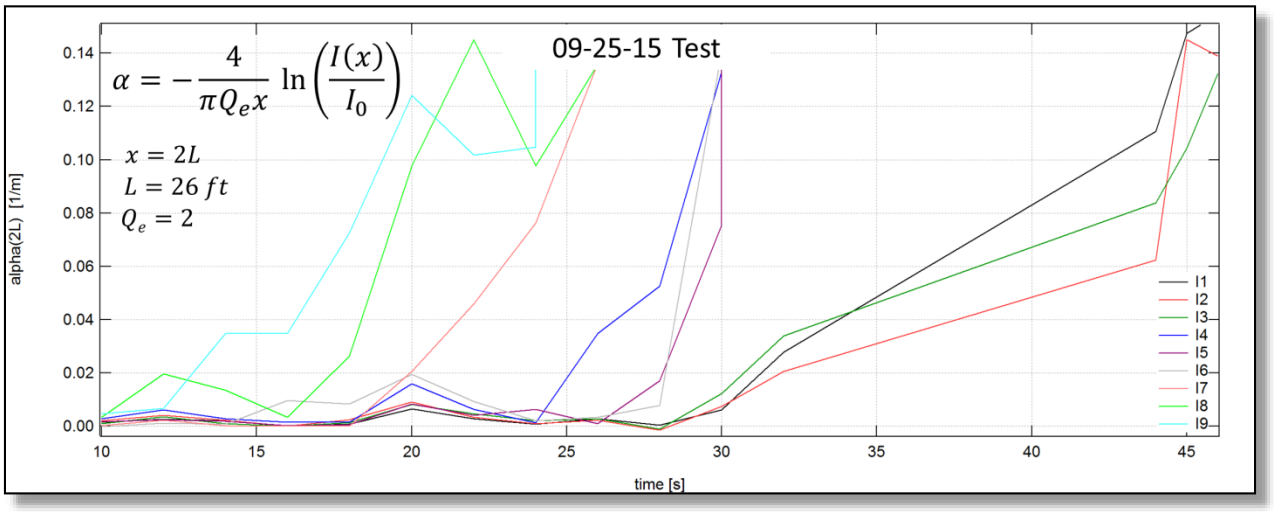

Fig. 9. Optical extinction factor of all 9 lasers in a 45 s test.

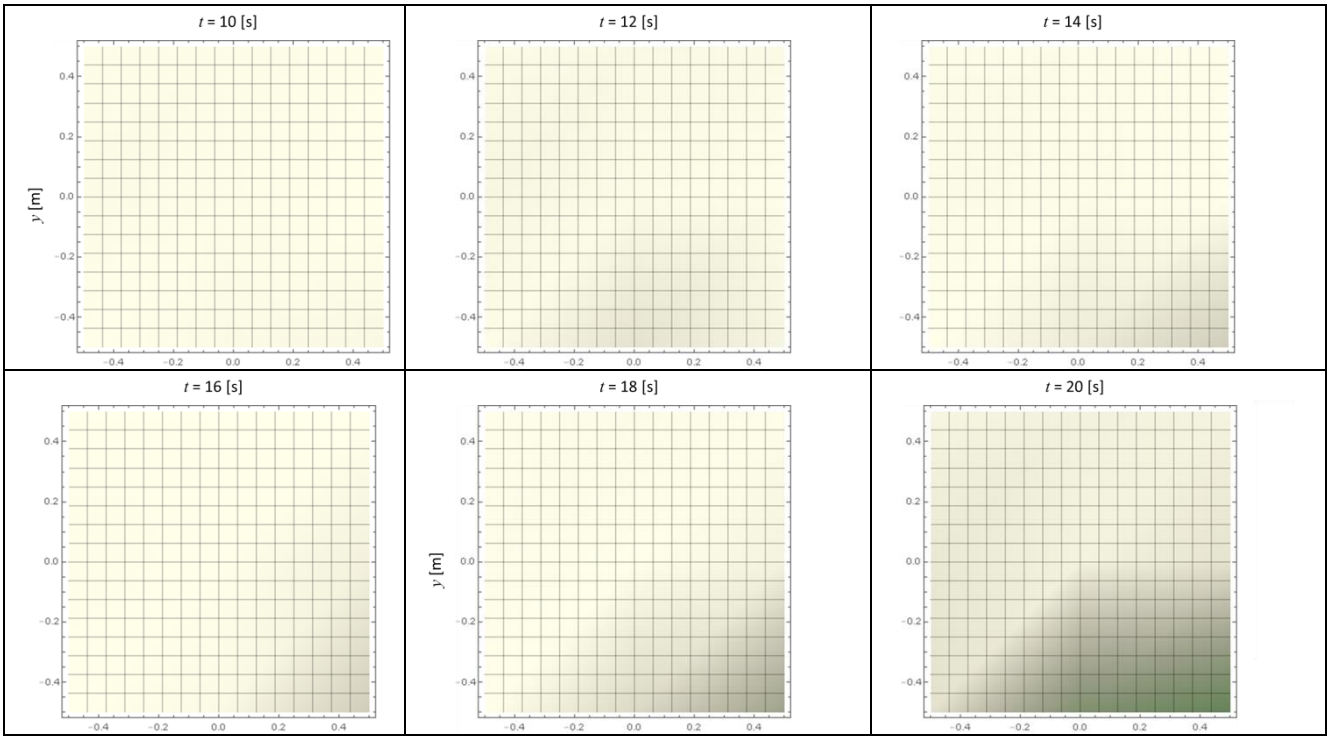

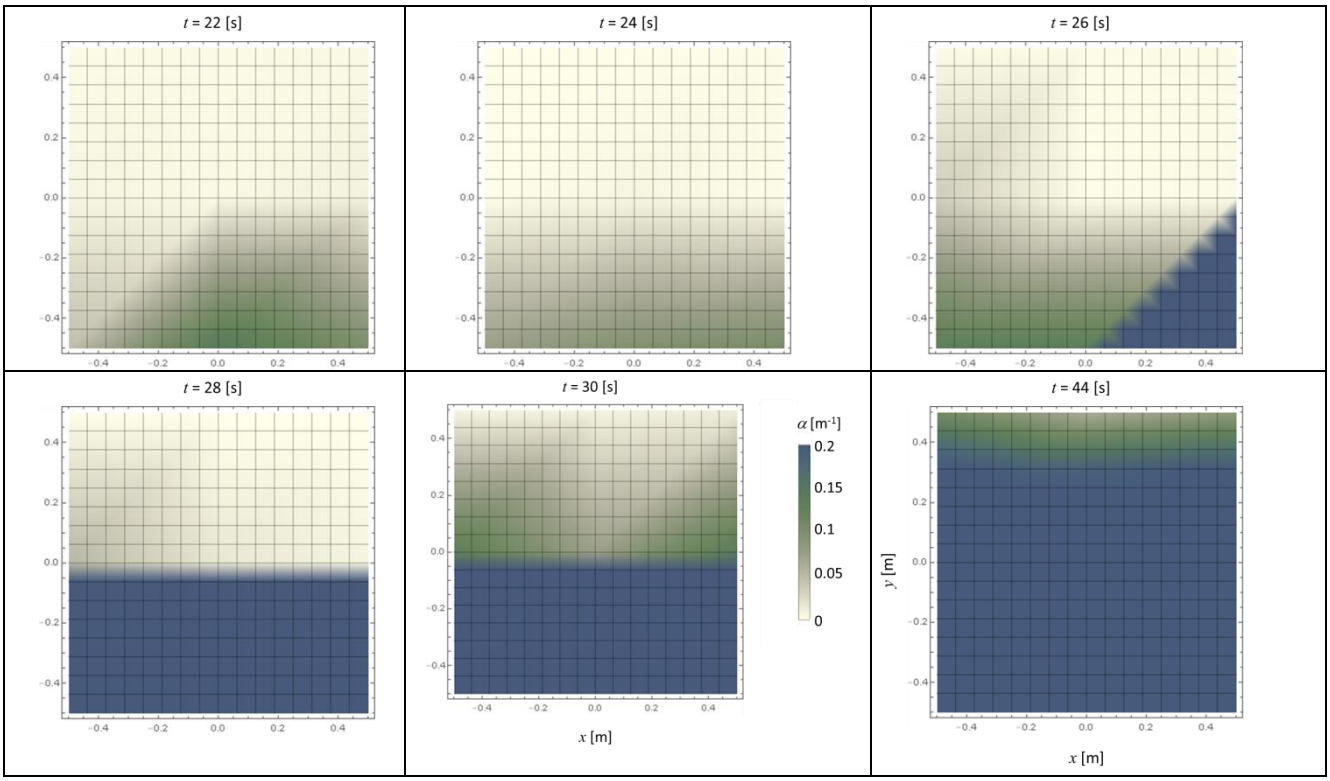

Fig. 10. 2D plots of dust density as it evolves over 45 s test.

SUMMARY AND DISCUSSION

Current technology development is underway at the GMRO Lab for telerobotic perception systems which may involve asteroid capture, Mars dust storms, and lunar regolith ISRU missions. A limitation of the current optical dust measurement system used in both the PRTB and the LRSB is due to the limited dynamic range of the image sensor, typically 8 bits, which has a theoretical dynamic range limit of just 48 dB. Current and future work involves enhancing and expanding the dynamic range of the dust measurement system based on the 8-bit (per RGB channel) image sensor of a COTS camera. Two methods are under investigation. The first method incorporate camera aperture and shutter speed (still camera) and image sensor gain and integration time (video camera) parameters into dust density measurement system. A combination of empirical models and data collection and analysis will provide the extended dynamic range (EDR) algorithm parameters. The accuracy of the EDR algorithm and increase in dynamic range will be quantified and verified. The second method, which is independent of or combined with the Phase I EDR algorithm, is side-scatter extinction measurements. This method has the added advantage of determining the dust density variation in a 3D space (at the cost of increased computational complexity). The outcome of this work is hoped to lead to improved planning and execution of robotic mining operations (terrestrial or extra-terrestrial) involving dust generating equipment, as well as improved operations of navigation and surveillance in dusty environments.

Acknowledgments. We gratefully acknowledge the work of Dr. Philip Metzger in the initial phase of this work.

REFERENCES

[1] Metzger, P. T., E. J. Lane, C. D. Immer, J. N. Gamsky, W. Hauslein, X. Li, R. C. Latta III, and C. M. Donahue (2010), Scaling of erosion rate in subsonic jet experiments and Apollo lunar module landings, paper presented at Earth and Space 2010, 12th Biennial Aerospace Division International Conference on Engineering, Construction and Operations in Challenging Environments, Am. Soc. of Civ. Eng., Honolulu, Hawaii.

[2] Cooper, BL, DS McKay, LM Riofrio, LA Taylor, and CP Gonzalez. 2010. Sub-10-micron and respirable particles in lunar soils. 41st Lunar and Planetary Science Conference – 2279.pdf.

[3] Goguen, JD. 2012. Apollo soils physical properties liked to M3 spectra combined with ROLO photometry. 43rd Lunar and Planetary Science Conference – 2568.pdf.

[4] Hapke, B. 2001. Space weathering from Mercury to the asteroid belt. J Geophysical Res. 106:10030-10073.

[5] Immer, C., P Metzger, PE Hintze, A Nick, and R Horan. 2011. Apollo 12 lunar module exhaust plume impingement on Lunar Surveyor III. Icarus 211: 1089-1102.

[6] Kiefer, HH, and TC Stone. 2005. The spectral irradiance of the Moon. The Astronomical Journal 129: 2887-2901.

[7] McClintock, WE, GM Holsclaw, MS Robinson, DT Blewett, DL Domingue, JW Head, NR Izenberg, EA Jensen, MC Kochte, MR Lankton, SL Murchie, AL Sprague, and F Vilas. 2008. Spectroscopic observations of Mercury's surface by the Mercury Atmospheric and Surface Composition Spectrometer during the first MESSENGER flyby. Lunar and Planetary Science XXXIX, 1330.pdf.

[8] Stark, C. 2006. Debayering demystified. AstroPhoto Insight Vol 2, 5-9. http://www.skyinsight.net/astrophoto/

[9] Lane, John E., and Philip T. Metzger. "Estimation of Apollo lunar dust transport using optical extinction measurements." Acta Geophysica 63.2 (2015): 568-599.